CSMA 2024
16ème Colloque National en Calcul des Structures
13-17 Mai 2024, Presqu'île de Giens (Var)

Adaptive computations on non-uniform grids by optimal transport in FFT-based homogenization

Cédric Bellis[1], Renaud Ferrier[2]

[1] *Aix Marseille Univ, CNRS, Centrale Marseille, LMA, Marseille, France, bellis@lma.cnrs-mrs.fr*
[2] *Mines Saint-Etienne, University of Lyon, CNRS, UMR 5307 LGF, Centre SMS, Saint-Etienne, France*

Résumé — This abstract focuses on the computation of a typical periodic cell problem that arises in homogenization. This model problem is intended to be discretized on a Fourier-basis and solved using a Fast Fourier Transform (FFT)-based iterative scheme. Such a method, which makes use of a uniform grid and global basis functions, has inherent limitations for correctly capturing any localized features of the solution, such as singularities or discontinuities. An adaptive method is proposed here to overcome these shortcomings, by allowing computations on a non-uniform grid.
Mots clés — Numerical homogenization, spectral method, *r*-adaptivity.

1 Introduction

The macroscopic properties of heterogeneous or microstructured media can efficiently be described and computed using homogenization methods. When the media are periodic, the numerical homogenization methods based on Fourier discretizations and the use of the Fast Fourier Transform (FFT) have shown to be very efficient since the seminal work [6]. Over the years, the latter have been successfully applied to a vast range of materials, with a variety of microstructure geometries and constitutive laws of the featured constituents. The performances of the underlying iterative algorithms have also been greatly improved to achieve faster convergence, see the review article [9]. Recently, an effort has been made to investigate quantitatively the behavior of solutions relatively to the spatial discretization and to establish convergence proofs for these numerical methods, see [1, 11, 10], as well as to develop a posteriori errors estimators [4].

When considering a periodic medium governed by a, possibly non-linear, local constitutive relation $\mathscr{C}$, then approximating the solution to a static or dynamic governing equation using the two-scale asymptotic homogenization method [7] leads to a cascade of cell problems posed on the characteristic periodic cell $\Omega_P \subset \mathbb{R}^d$. These problems all have the same structure and boil down, in acoustics, electromagnetism or elasticity, to the following generic static problem, see e.g. [3] :

$$\text{Find } \boldsymbol{u} \in H^1_{\text{per}}(\Omega_P) \text{ such that } \begin{cases} \boldsymbol{s}(\boldsymbol{x}) = \mathscr{C}\big(\boldsymbol{x}, \boldsymbol{g}_0 + \operatorname{grad} \boldsymbol{u}\big), \\ \operatorname{div} \boldsymbol{s}(\boldsymbol{x}) + \boldsymbol{h}(\boldsymbol{x}) = \boldsymbol{0}, \\ \langle \boldsymbol{u} \rangle_{\Omega_P} = \boldsymbol{0}. \end{cases} \tag{1}$$

For any domain Ω with associated spatial variable $\boldsymbol{\zeta}$, the averaging operator $\langle \cdot \rangle_\Omega$ is defined as

$$\langle \beta \rangle_\Omega = \frac{1}{|\Omega|} \int_\Omega \beta(\boldsymbol{\zeta}) \, \mathrm{d}\boldsymbol{\zeta}. \tag{2}$$

In computational homogenization we deal with heterogeneous media that are often composites materials with discontinuous constitutive properties. This results in sharp material interfaces and, possibly, geometrical corners that in turn induce discontinuities or singularities in the Partial Differential Equation (PDE) solutions. The latter are notoriously difficult to capture accurately using Fourier spectral methods, which make use of uniform computational meshes or grids. As a consequence, it may be critical to adapt the computations for such configurations and solutions as a lack of accuracy in the local fields can in turn impact the accuracy of the targeted homogenized properties.

To do so, our approach will be twofold :
(i) Compute a geometrical mapping that redistributes the points of a uniform computational grid according to a desired density, typically concentrating grid points in the original physical domain where a greater accuracy is required. This amounts to a *r*-adaptation strategy, i.e. a remeshing or relocation method.
(ii) Transport the PDE considered from the physical domain, by now discretized on a non-uniform grid, to the computational domain where it can ultimately be solved on a uniform grid, using standard FFT-based numerical schemes.

2 Geometrical mapping

The solution $\boldsymbol{u}$ to (1) is known to be not well-behaved in the regions where the constitutive relation $\mathscr{C}$ involves discontinuous parameters, exhibiting large gradients that make it difficult to approximate accurately on regular grids. Therefore, achieving high-accuracy with a given number of degrees of freedom requires an adapted discretization that is *non-uniform* in space. With this issue in mind, the points $\boldsymbol{x}$ in (1) are thought of as the points of a non-uniform discretization grid covering the physical domain Ω_P.

In this context, we consider a mapping of the periodic cell Ω_P to a computational domain Ω_C, which is intended to be discretized using a *uniform* grid. Doing so, the computations on Ω_C can be performed efficiently using FFT toolboxes. To do so, we introduce an invertible and sufficiently smooth non-homogeneous transformation $\boldsymbol{\varphi}$ such that

$$\boldsymbol{x} = \boldsymbol{\varphi}(\boldsymbol{X}). \tag{3}$$

The gradient of $\boldsymbol{\varphi}$ is the invertible second-order tensor $\boldsymbol{F}$, which can be represented as the Jacobian matrix of the transformation, defined locally as :

$$\boldsymbol{F}(\boldsymbol{X}) = \frac{\partial \boldsymbol{\varphi}(\boldsymbol{X})}{\partial \boldsymbol{X}} = \frac{\partial \boldsymbol{x}}{\partial \boldsymbol{X}}. \tag{4}$$

In addition, the Jacobian J of the transformation is defined as

$$J(\boldsymbol{X}) = \det \boldsymbol{F}(\boldsymbol{X}).$$

The mapping of fields between the two domains is achieved as follows : Let $\boldsymbol{t}$ be a (tensor) field on Ω_P then we associate it with a field $\boldsymbol{T}$ defined on Ω_C as

$$\boldsymbol{T}(\boldsymbol{X}) = \boldsymbol{t}(\boldsymbol{\varphi}(\boldsymbol{X})) = \boldsymbol{t}(\boldsymbol{x}),$$

which defines a smooth mapping $\boldsymbol{t} = \Phi(\boldsymbol{T})$. In the following, lowercase (resp. uppercase) letters will be employed to denote quantities expressed on Ω_P (resp. Ω_C) according to the mapping Φ.

With the purpose of transporting a given system of PDEs formulated on the physical problem Ω_P to the computational domain Ω_C we now address the transformation rules for differential operators. Upon introducing the gradient and divergence operators Grad and Div relatively to the variable $\boldsymbol{X}$, then the chain rules can be used so as to obtain the following result :

$$\operatorname{grad} \boldsymbol{t}(\boldsymbol{x}) = \operatorname{Grad} \boldsymbol{T}(\boldsymbol{X}) \cdot \boldsymbol{F}^{-1} \qquad \text{and} \qquad \operatorname{div} \boldsymbol{t}(\boldsymbol{x}) = \frac{1}{J} \operatorname{Div} \left(\boldsymbol{T}(\boldsymbol{X}) \cdot J\boldsymbol{F}^{-T} \right).$$

3 Optimal transport-based coordinate mapping

3.1 Problem formulation.

In a general geometrical setting, we adopt a strategy based on optimal transport, which provides a rational framework well-suited to the grid adaptation problem. It amounts to defining some *strictly positive* source and target densities s and t, respectively in Ω_C and Ω_P, and finding the optimal transport map $\boldsymbol{\varphi}$ between them that minimizes a given cost. In the case where the cost is defined as the discrepancy to the identity map in the L^2-norm then this problem can be interpreted as the Monge–Kantorovich mass

transfer problem, see e.g. [8]. When the densities are smooth, it is well-known [2] that the sought optimal transport map $\boldsymbol{\varphi}$ can be written as the gradient of a convex potential ψ and is the unique solution to

$$t\big(\boldsymbol{x}(\boldsymbol{X})\big)J(\boldsymbol{X}) = s(\boldsymbol{X}) \quad \text{with} \quad \boldsymbol{x} = \boldsymbol{\varphi}(\boldsymbol{X}) \stackrel{\text{def}}{=} \operatorname{Grad}\psi(\boldsymbol{X}). \tag{5}$$

The problem (5) can be simply interpreted as this of finding the (optimal) mapping $\boldsymbol{\varphi}$ that redistributes the source density s in the computational domain Ω_C to the target density t in the physical domain Ω_P.

Using that $J(\boldsymbol{X}) = \det(\partial\boldsymbol{\varphi}(\boldsymbol{X})/\partial\boldsymbol{X})$, the problem (5) can be directly formulated in terms of the convex potential ψ, which leads to the Monge-Ampère equation :

$$t\big(\operatorname{Grad}\psi(\boldsymbol{X})\big)\det\big(H\psi(\boldsymbol{X})\big) = s(\boldsymbol{X}), \tag{6}$$

where H is the Hessian operator, i.e. $H\psi(\boldsymbol{X}) = \operatorname{Grad}\operatorname{Grad}\psi(\boldsymbol{X})$.

3.2 Proposed algorithm.

In the case considered of periodic boundary conditions and positive, smooth and periodic source and target densities s and t, the problem (6) is rewritten as follows [5] : define the functional f of periodic (scalar) potentials ϕ as

$$f(\phi) : \boldsymbol{X} \mapsto t\big(\boldsymbol{X} + \operatorname{Grad}\phi(\boldsymbol{X})\big)\det\big(\boldsymbol{I} + H\phi(\boldsymbol{X})\big) - s(\boldsymbol{X}), \tag{7}$$

and find ϕ such that

$$f(\phi) = 0 \quad \text{with} \quad \psi : \boldsymbol{X} \mapsto \frac{|\boldsymbol{X}|^2}{2} + \phi(\boldsymbol{X}) \text{ convex}. \tag{8}$$

To perform a Newton iteration on the equation (8) we linearize f as $f(\phi + h\tilde{\phi}) = f(\phi) + hDf(\phi)\cdot\tilde{\phi} + o(h)$. Given ϕ_n, we then intent to perform quasi-Newton iterations by computing the solution $\tilde{\phi}$ to an *approximate* linearized equation $Df(\phi_n)\cdot\tilde{\phi} = -f(\phi_n)$.

3.3 Example of an a posteriori adaptation

Consider first the solution $\boldsymbol{u}$ to the problem (1) with $\mathscr{C}$ linear, using $\boldsymbol{h} = \boldsymbol{0}$ and a loading arbitrarily defined as $\boldsymbol{g}_0 = (1,0)$ for the sake of the example. This solution can be computed on a preliminary regular coarse grid in Ω_P (which can be different from the computational grid ultimately used in Ω_C). This solution is relatively smooth, unlike its gradient, which can be computed in Fourier space. Then, a target density function can be computed from there by smoothing the local Euclidean norm of the gradient $\mathcal{G}\|\operatorname{grad}\boldsymbol{u}\|_2(\boldsymbol{x})$, and applying a suitable scaling and normalization. An adapted grid obtained for a random circular inclusions problem is shown in Figure 1.

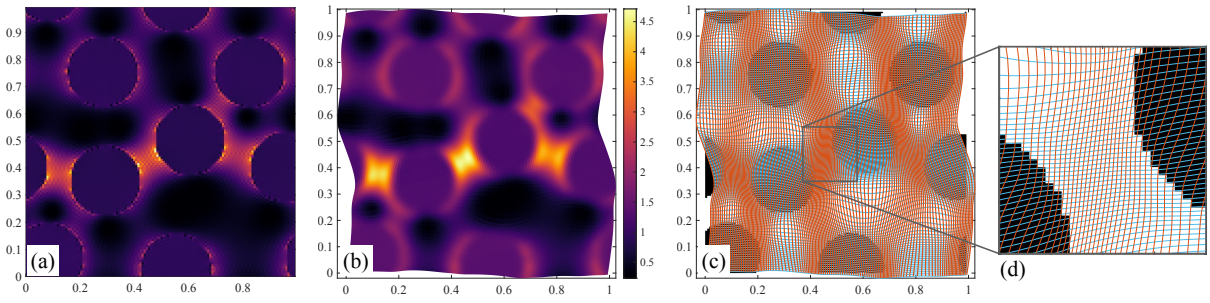

FIGURE 1 – Grid adaptation for a random circular inclusions problem based on the computation of a preliminary solution $\boldsymbol{u}$: (a) Euclidean norm $\|\operatorname{grad}\boldsymbol{u}\|_2(\boldsymbol{x})$, (b) target density function $t(\boldsymbol{x})$, (c) adapted grid (red/blue), (d) close-up.

4 Transported cell problem

Owing to the results in Section 2, the generic cell problem (1) when transported from Ω_P to Ω_C reads :

$$\text{Find } \boldsymbol{U} \in H^1_{\text{per}}(\Omega_C) \text{ such that } \begin{cases} \boldsymbol{S}(\boldsymbol{X}) = \mathscr{C}\big(\boldsymbol{\varphi}(\boldsymbol{X}), \boldsymbol{G}_0 + \text{Grad}\,\boldsymbol{U} \cdot \boldsymbol{F}^{-1}\big), \\ \text{Div}\,\big(\boldsymbol{S}(\boldsymbol{X}) \cdot J(\boldsymbol{X}) \boldsymbol{F}^{-T}(\boldsymbol{X})\big) + J(\boldsymbol{X}) \boldsymbol{H}(\boldsymbol{X}) = \boldsymbol{0}, \\ \overline{\boldsymbol{U}} = \boldsymbol{0}. \end{cases} \tag{9}$$

In the problem above, the transformed mean value $\overline{\boldsymbol{U}}$ is defined as

$$\overline{\boldsymbol{U}} = \left(\int_{\Omega_C} J(\boldsymbol{X})\, \mathrm{d}\boldsymbol{X} \right)^{-1} \int_{\Omega_C} \boldsymbol{U}(\boldsymbol{X}) J(\boldsymbol{X})\, \mathrm{d}\boldsymbol{X} = \frac{\langle \boldsymbol{U} J \rangle_{\Omega_C}}{\langle J \rangle_{\Omega_C}}. \tag{10}$$

To solve the problem (9) formulated on the uniformly discretized computational domain Ω_C then standard FFT-based approaches can be adopted, namely fixed-point or gradient-based algorithms, see e.g. [6]. To do so, one introduces the periodic gradient Green's operator $\widetilde{\widetilde{\boldsymbol{\Gamma}}}_0 : L^2_{\text{per}}(\Omega_C) \to L^2_{\text{per},0}(\Omega_C)$, relatively to a linear comparison medium $\boldsymbol{C}_0$. Here, $L^2_{\text{per}}(\Omega_C)$ is the space of Ω_C-periodic, not necessarily symmetric, tensor-valued fields that are square-integrable, and $L^2_{\text{per},0}(\Omega_C)$ its subspace of zero-mean fields. Then we make use of the following fixed-point scheme for all point $\boldsymbol{X}$ of a uniform grid discretizing Ω_C :

$$\begin{cases} \text{Grad}\,\boldsymbol{U}^{(0)}(\boldsymbol{X}) = \boldsymbol{0}, \\ \text{Grad}\,\boldsymbol{U}^{(n+1)}(\boldsymbol{X}) = \text{Grad}\,\boldsymbol{U}^{(n)}(\boldsymbol{X}) - \Big[\widetilde{\boldsymbol{\Gamma}}_0 \widetilde{\boldsymbol{C}} \Big(\widetilde{\boldsymbol{G}}_0 + \text{Grad}\,\boldsymbol{U}^{(n)} \Big) \Big] (\boldsymbol{X}), \end{cases} \tag{11}$$

where we have introduce a *virtual* constitutive tensor $\widetilde{\boldsymbol{C}}$ (here in the linear case) and a *virtual* source term $\widetilde{\boldsymbol{G}}_0$ on Ω_C . Note that the reference medium $\boldsymbol{C}_0$ has to be chosen so as to ensure convergence of (11).

5 Numerical results

5.1 Full-field comparison

The geometry of the random circular inclusions in Figure 1 is considered. The adapted grid is computed using the solution-based approach in Fig. 1. Doing so, grid points are concentrated in the regions where a preliminary solution computed on a regular grid exhibits strong gradients. Full anisotropy and an increase in the (virtual) material contrast are obtained, but here the inclusions are also distorted in the computational domain Ω_C due to the heterogeneity of the mapping.

The solution to (1) is then computed, both on a regular grid in Fig. 2(a-b), and on the adapted grid in Fig. 2(c-d). While these two simulations are comparable for this configuration, the adapted computation is *qualitatively* more satisfying, with a solution being smoother than the one computed on the regular grid at the same discretization, and with discontinuities being better captured. Quantitative comparisons and convergence analysis are investigated in the next section.

5.2 Convergence results

In this section we investigate the convergence properties of the adaptive computations relatively to the discretization parameter N, the 2D computational grid being of $N \times N$ pixels. The material contrast is set to $z = 10$ and the conjugate gradient method is used for these computations. We use the effective parameters as quantitative metrics to assess the performance of the proposed method.To do so, consider the effective energy W_{eff} defined as

$$W_{\text{eff}}(\boldsymbol{g}_0) = \min_{\boldsymbol{e}_* = \text{grad}\,\boldsymbol{w}} \big\langle w(\boldsymbol{x}, \boldsymbol{g}_0 + \boldsymbol{e}_*) \big\rangle_{\Omega_P} \tag{12}$$

in terms of the local energy density w associated with the problem (1) considered. For the adaptive computation, the averaged energy in the equation above is directly computed in the computational domain

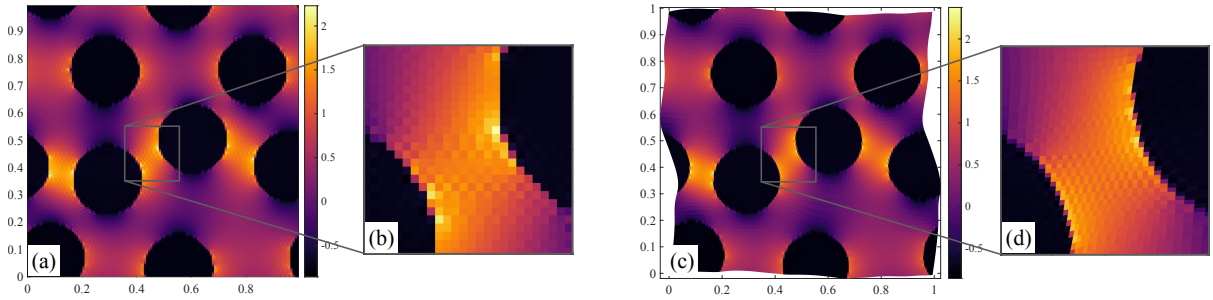

FIGURE 2 – Random circular inclusions : comparison of the first component of the solution $\operatorname{grad} \boldsymbol{u}(\boldsymbol{x})$ to (1) in Ω_P computed using (a) a regular grid and (c) the adapted grid of Fig. 1, with close-ups in (b) and (d), respectively.

Ω_C using the transformation rules :

$$\begin{aligned} \big\langle w(\boldsymbol{x}, \boldsymbol{g}_0 + \operatorname{grad} \boldsymbol{w}) \big\rangle_{\Omega_P} &= \frac{1}{|\Omega_P|} \int_{\Omega_P} w(\boldsymbol{x}, \boldsymbol{g}_0 + \operatorname{grad} \boldsymbol{w}) \, \mathrm{d}\boldsymbol{x} \\ &= \frac{1}{|\Omega_P|} \int_{\Omega_C} w(\boldsymbol{\varphi}(\boldsymbol{X}), \boldsymbol{G}_0 + \operatorname{Grad} \boldsymbol{W} \cdot \boldsymbol{F}^{-1}) J(\boldsymbol{X}) \, \mathrm{d}\boldsymbol{X}. \end{aligned} \tag{13}$$

From (12) and (13) one can then extract some effective parameters depending on the choice of the applied macroscopic gradient $\boldsymbol{g}_0$. It is worth noting that, as is standard practice in FFT-based methods, the averaging operator $\langle \cdot \rangle_{\Omega_C}$ is computed using the trapezoidal rule on the regular FFT grid.

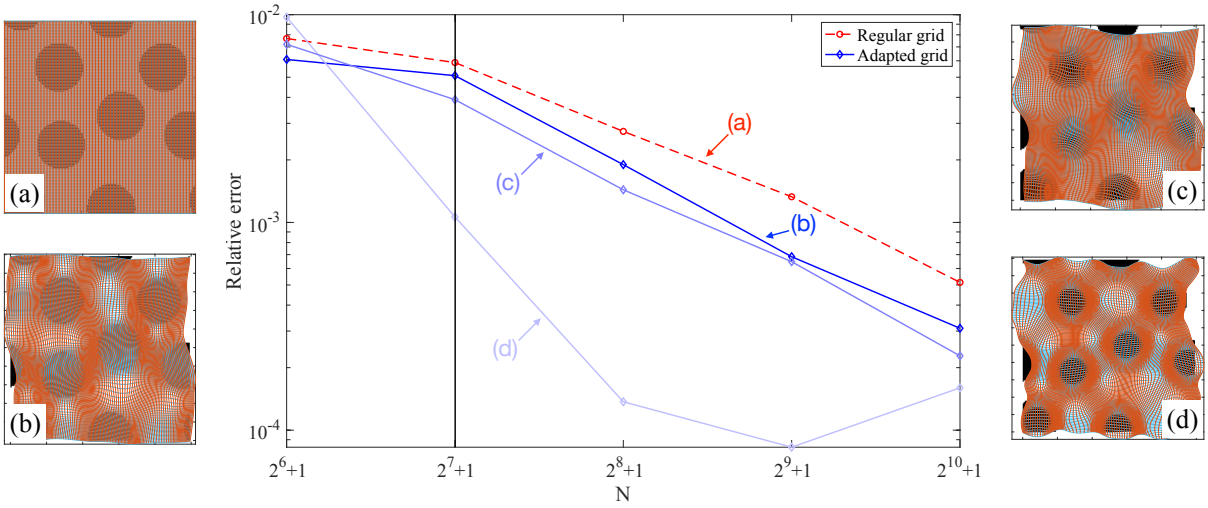

FIGURE 3 – Random circular inclusions : comparison of the relative errors on the effective parameter computed using a regular grid (a) and adapted ones (b,c,d), as functions of the discretization parameter N (horizontal axis is in log base 2 scale). For the grids on the left and $N = 2^7 + 1$ see fields comparison in Fig. 2.

A convergence analysis relatively to the discretization parameter is performed in the random circular inclusions case. Here, errors are computed relatively to a simulation on a regular grid with $N = 2^{12} + 1$ pixels. The obtained results are synthesized in Figure 3 where, for the geometry considered, the adaptive method is deployed using the solution-based approach that leads to Figure 1 (dark blue curve and panel b) and which has been investigated previously. The panels (c) and (d) correspond to grid adaptations using the distance to the closest inclusion or the detection of interfaces, respectively. For the mapping in (b), a systematic gain in accuracy is highlighted in Fig. 3 using the adapted grid compared to the regular one. The improvement corresponds here to a reduction between 13.5% to 48.6% for the discretizations considered, making the proposed approach interesting to improve the overall quality of the simulation. For completeness, the convergence behavior has also been quantified for other coordinate mappings, see grids (c,d) and light blue curves. In such cases, precision gains are nearly systematic and sometimes quite significant.

6 Conclusion

To conclude, the proposed adaptive Fourier spectral method can be used to improve the accuracy of a numerical approximation computed on a regular grid, provided that the monitor function is adequately defined. It easily amenable to common FFT-based platforms as it is minimally intrusive : its implementation only necessitates (i) the computation of the Monge–Ampère equation, a problem set in divergence form, (ii) the introduction of the virtual constitutive relation and source terms, and (iii) a minor modification of the Green's tensor.

Références

[1] Cédric Bellis, Hervé Moulinec, and Pierre Suquet. Eigendecomposition-based convergence analysis of the neumann series for laminated composites and discretization error estimation. *International Journal for Numerical Methods in Engineering*, 121(2) :201–232, 2020.

[2] Y. Brenier. Polar factorization and monotone rearrangement of vector-valued functions. *Communications on Pure and Applied Mathematics*, 44(4) :375–417, 1991.

[3] Rémi Cornaggia and Cédric Bellis. Tuning effective dynamical properties of periodic media by FFT-accelerated topological optimization. *International Journal for Numerical Methods in Engineering*, 121(14) :3178–3205, 2020.

[4] Renaud Ferrier and Cédric Bellis. A posteriori error estimations and convergence criteria in fast Fourier transform-based computational homogenization. *International Journal for Numerical Methods in Engineering*, 124(4) :834–863, 2023.

[5] Grégoire Loeper and Francesca Rapetti. Numerical solution of the Monge–Ampère equation by a Newton's algorithm. *Comptes Rendus Mathematique*, 340(4) :319–324, 2005.

[6] H. Moulinec and P. Suquet. A numerical method for computing the overall response of nonlinear composites with complex microstructure. *Comp. Meth. Appl. Mech. Engng.*, 157 :69–94, 1998.

[7] E Sanchez-Palencia. *Non-Homogeneous Media and Vibration Theory*. Springer, Berlin, Heidelberg, 1978.

[8] Filippo Santambrogio. *Optimal Transport for Applied Mathematicians*. Birkhäuser, 2015.

[9] Matti Schneider. A review of nonlinear FFT-based computational homogenization methods. *Acta Mechanica*, 232(6) :2051–2100, 2021.

[10] Matti Schneider. On the effectiveness of the Moulinec–Suquet discretization for composite materials. *International Journal for Numerical Methods in Engineering*, 124(14) :3191–3218, 2023.

[11] C. Ye and E.T. Chung. Convergence of trigonometric and finite-difference discretization schemes for FFT-based computational micromechanics. *BIT Numer. Math.*, 63 :11, 2023.